

Chapter 4

Ultra-small mode volume Si-Ag core-shell nanowire resonators

4.1 Introduction

Until recently, any advances in the field of optics have been limited by diffraction. This restricts the size of all optical components to dimensions larger than half the wavelength of light it supports. The field of plasmonics has emerged with the unique ability to confine optical waveguide and resonator modes to volumes well below the diffraction limit. The extremely high and localized fields in these plasmonic nanocavities are finding applications in research areas such as single-molecule sensing, nanowire lasers, and fluorescence enhancement, among others. Plasmonic resonators, although they generally have low quality factors Q , are able to confine modes to subwavelength volumes V . Thus, when considering as a figure of merit the quantity Q/V , plasmonic structures become much more competitive with conventional optical resonators for applications where a resonance confined to a small volume is desirable.

Conventional dielectric resonators are renowned for their exceptionally high quality factors. For example, the silica toroid microcavity exhibits a Q of 4×10^8 , but with a large mode volume of $160(\lambda/n)^3$, where λ is the free space wavelength and n is the refractive index of the dielectric [64]. Taking advantage of the high confinement within plasmonic nanocavities, metallodielectric devices can be designed to support modes at subwavelength volumes. One of the most intensely studied plasmonic structures exhibiting high modal confinement over microns of propagation is the planar metal-insulator-metal (MIM) waveguide. An MIM cavity 107 nm wide

and 3 μm long with a 14 nm SiO_2 slot in Au has experimentally demonstrated mode volumes as small as $0.00383(\lambda/n)^3$ [13]. We have chosen to take advantage of the high confinement and low loss in MIM cavities in a cylindrical geometry as the core-shell nanowire resonator. These resonators are structures consisting of a cylindrical semiconductor or dielectric core and concentric metallic cladding (Figure 4.1). The core-shell resonator materials system explored here is a Si nanowire surrounded by an optically thick Ag cladding.

In this chapter, we demonstrate that plasmonic core-shell nanowire resonators confine modes to deeply subwavelength volumes while maintaining reasonable quality factors in extremely small structures. We use the boundary element method (BEM) to investigate Si-Ag core-shell nanowire resonators with a variety of dimensions, and for the resonant modes supported in each structure we determine the local density of states (LDOS), two-dimensional near-field intensity mode profiles, effective mode volume V , and quality factor Q . Additionally, we show that this geometry is well suited to obtain large Purcell factors and enhance the rate of spontaneous emission.

4.2 Resonant Modes of Si-Ag Core-Shell Nanowire Resonators

We investigate plasmonic core-shell nanowire resonators consisting of a Si nanowire core surrounded by an optically thick Ag cladding, shown schematically in Figure 4.1. These structures are defined by a core radius a , length L , and have a constant Ag coating thickness $T = 100$ nm. We use the boundary element method (BEM) to investigate resonators with a variety of dimensions, and for each mode we determine the LDOS, effective mode volume (V_{eff}), quality factor (Q), and enhancements in the total and radiative decay rates (Γ_{tot} and Γ_{rad} , respectively, normalized to decay in vacuum, Γ_0), and the corresponding quantum efficiency $\eta = \Gamma_{\text{rad}}/\Gamma_{\text{tot}}$.

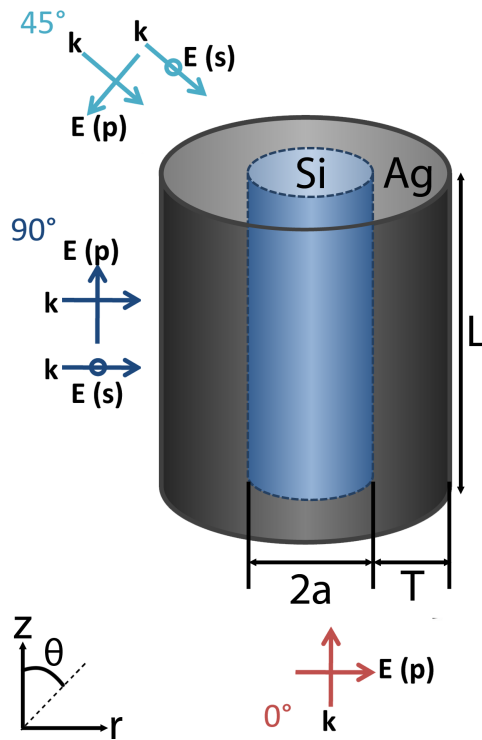


Figure 4.1. Si-Ag core-shell nanowire resonator, consisting of a Si core (radius a), Ag cladding (thickness T), and length L . Orientations for plane-wave excitation at $\theta = 0^\circ$, $\theta = 45^\circ$, and $\theta = 90^\circ$ (s - and p -polarized) are shown.

4.2.1 The Boundary Element Method

In BEM, calculations are performed in the frequency domain with the electromagnetic field in each homogeneous region expressed as a function of auxiliary boundary charges and currents. After applying boundary conditions, a set of linear integrals is obtained and solved by discretization. The axial symmetry of core-shell nanowire resonators allows decomposition of the fields into uncoupled azimuthal components m with azimuthal angular dependence $e^{im\phi}$. This results in an essentially a one-dimensional field calculation that is solved with great accuracy. The dielectric functions of Si and Ag are input using tabulated data. Converged results are found for $m_{\max} = 3$, using values of m defined by

$$m = -m_{\max}, -m_{\max} + 1, \dots, m_{\max} - 1, m_{\max}. \quad (4.1)$$

Resonant modes are determined by calculating the LDOS ρ for a dipole emitter oriented along the x direction using the relation

$$\rho = \frac{\omega^2 n}{3\pi^2 c^3} + \frac{1}{2\pi^2 \omega} \text{Im}[E_{\text{ind}}/D], \quad (4.2)$$

where ω is the resonance frequency, c is the speed of light in vacuum, n is the refractive index of Si, D is the dipole strength (unity in BEM), and E_{ind} is the contribution to the electric field due to scattering at the interfaces and projected along the direction of polarization. In contrast to the electronic density of states that describes the number of *electron* states at a given energy level that are available to be occupied, the LDOS counts the number of electromagnetic, or *photon*, states at a given frequency, location, and orientation of a dipole emitter. From (4.2), it is obvious that the LDOS depends on frequency, position, and orientation. The resonance quality factor, Q , is determined by fitting a Lorentzian lineshape to a plot of ρ versus ω , and

$$Q = \frac{\omega}{\Delta\omega}, \quad (4.3)$$

where $\Delta\omega$ is the full width at half maximum.

We use plane-wave excitation incident at $\theta = 0^\circ$, polarized along an arbitrary radial direction (see Figure 4.1), and determine the spatial near-field intensity profiles $|\mathbf{E}|^2$ of each mode. The effective mode volume, V_{eff} , is defined as a cylinder with length L_{eff} and radius a_{eff} determined by the $1/e$ decay distance of the peak field intensity inside the Si core.

4.2.2 Longitudinal Modes of Core-Shell Nanowire Resonators

If we consider a simple resonator cavity consisting of two parallel mirrors separated by a length L , basic optics tells us that a number of standing waves (modes) will be supported at wavelengths that satisfy the constraint $L = m\lambda/2$, where m is an integer. This is illustrated schematically in Figure 4.2, showing the modes at $\lambda = 2L$, $\lambda = L$, $\lambda = 2L/3$, and $\lambda = L/4$ illustrated here. Similarly, in a plasmonic cavity such as the core-shell nanowire resonator in the bottom of Figure 4.2, a number of longitudinal resonances are supported inside the Si core. However, plasmonic modes access larger k -vectors (shorter wavelengths).

Figure 4.3 shows LDOS calculations of the longitudinal resonances for four different Si-Ag core-shell nanowire resonators. The LDOS is calculated at a constant radial position of $r = 5$ nm from the center of the Si core, along the length of the wire, and reported with values normalized to the vacuum LDOS. The largest resonator (Figure 4.3a) has a core radius $a = 50$ nm and length $L = 500$ nm. A number of modes are supported, with the lowest-order $\lambda/2$ resonance occurring near $\lambda = 1000$ nm. Modes with higher-order azimuthal symmetry are supported at wavelengths below $\lambda = 750$ nm. Keeping the same Si core radius but decreasing the length to $L = 150$ nm, these higher order modes are cut off (Figure 4.3b). As expected, fewer longitudinal resonances are supported. The lowest-order $\lambda/2$ resonance, characterized by a high LDOS in the center of the resonator, has a resonant wavelength very close to the longer resonator in Figure 4.3a, but the second $\lambda/2$ resonance shifts from $\lambda = 980$ nm to $\lambda = 800$ nm. Also notable is that the lowest-order mode has higher LDOS in the smaller resonator.

Decreasing the resonator core radius a has a more marked effect on the wavelength

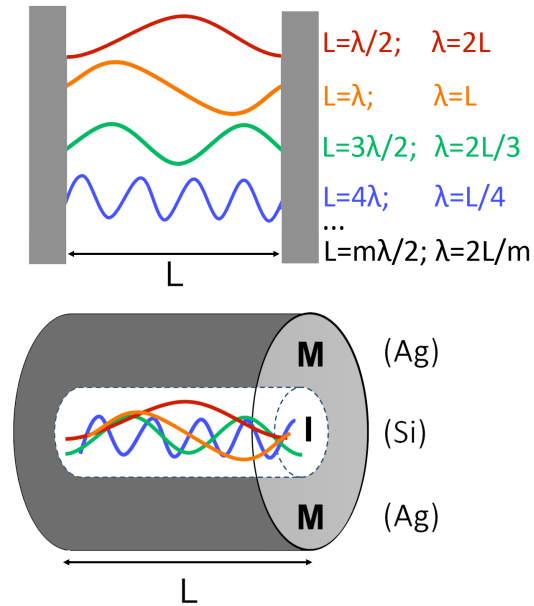


Figure 4.2. Top: Longitudinal modes of a resonator consisting of two parallel mirrors in vacuum separated by a distance L . Modes are supported at wavelengths that satisfy the constraint $L = m\lambda/2$, where m is an integer, with modes at $\lambda = 2L$, $\lambda = L$, $\lambda = 2L/3$, and $\lambda = L/4$ illustrated here. Bottom: Similar longitudinal mode profiles are found inside a Si-Ag core-shell nanowire resonator, at wavelengths much shorter than their free-space counterpart.

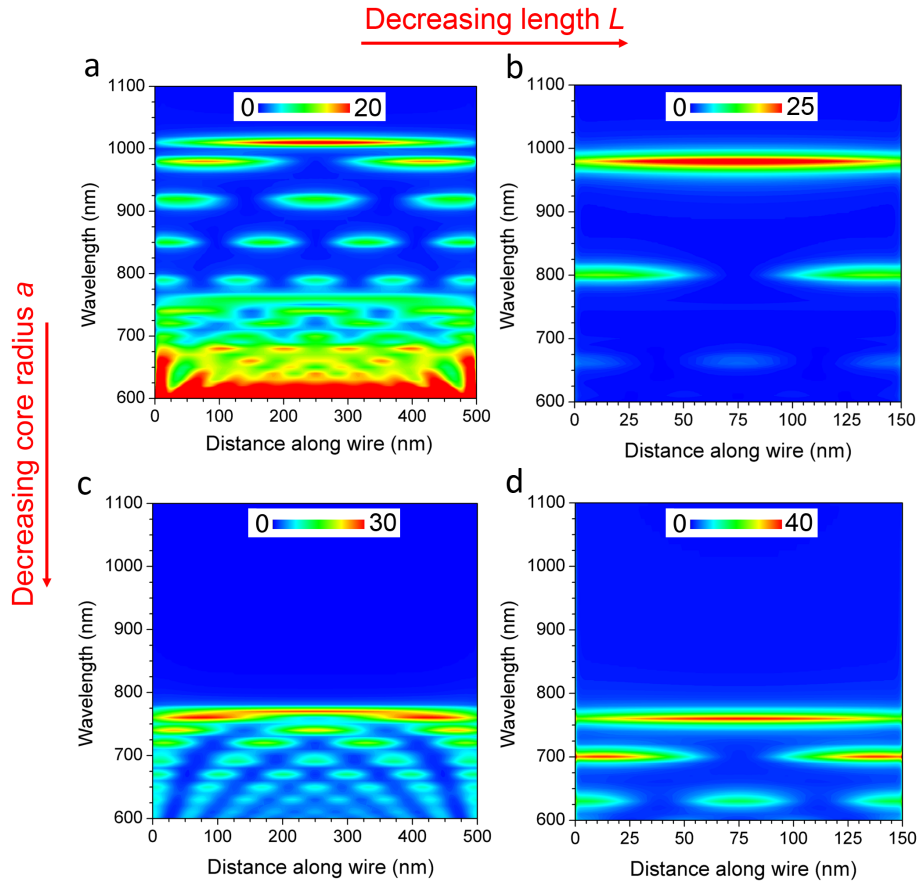


Figure 4.3. LDOS as a function of distance along the resonator length (z -axis) and wavelength for modes of Si-Ag core-shell nanowire resonators with dimensions (a) $a = 50$ nm, $L = 500$ nm, (b) $a = 50$ nm, $L = 150$ nm, (c) $a = 25$ nm, $L = 500$ nm, and (d) $a = 25$ nm, $L = 150$ nm. The LDOS is calculated at a constant radial position of $r = 5$ nm from the center of the Si core, along the length of the wire, and reported with values normalized to the vacuum LDOS. As length L decreases, fewer longitudinal modes are supported. As core radius decreases, modes shift to shorter wavelengths.

of the lowest-order longitudinal resonance. Comparing the modes of a resonator with $L = 500$ nm and $a = 50$ nm (Figure 4.3a) to a resonator of the same length but smaller radius $a = 25$ nm (Figure 4.3c), we can see that a similar number of longitudinal resonances are supported, but pushed to shorter wavelengths and spaced closer together spectrally. Furthermore, the higher-order azimuthal resonances in the larger resonator are not supported in the smaller structure. Again, this smaller resonator exhibits higher LDOS intensities than the larger structure.

Comparing the shorter resonators in Figs 4.3b ($L = 150$ nm, $a = 50$ nm) and 4.3d ($L = 150$ nm, $a = 25$ nm), similar trends are observed. The smaller resonator supports the same longitudinal resonances but at shorter wavelengths. Most importantly, the highest LDOS is seen in the smallest resonator. In Section 4.3, the modes of the resonators in Figures 4.3a and 4.3d are discussed in more depth.

4.3 A Case Study: 3 Resonators, 3 Size Regimes

Detailed results are presented for three resonators, each representing a different size regime: A ($a = 50$ nm, $L = 500$ nm, $T = 100$ nm), B ($a = 25$ nm, $L = 150$ nm, $T = 100$ nm), and C ($a = 5$ nm, $L = 25$ nm, $T = 100$ nm). Data for the largest resonator (A) are seen in Figure 4.4. The LDOS (Figure 4.4b) and NF $|\mathbf{E}|^2$ from plane wave excitation at $\theta = 0^\circ$ (Figure 4.4c) are calculated at a specific radial position ($r = 5$ nm from the center of the Si core) and plotted as a function of wavelength λ and distance along the wire. Many modes are supported, with the lowest-order $\lambda/2$ resonance occurring at $\lambda = 1010$ nm. Modes with similar longitudinal profiles but higher-order azimuthal dependence appear at shorter wavelengths in the LDOS plot, but symmetry prevents these modes from excitation with plane waves and they are not apparent in Figure 4.4c.

Two-dimensional NF $|\mathbf{E}|^2$ cross-sectional profiles of the first four lowest-order longitudinal resonances of resonator A are shown in Figure 4.5. The modes at $\lambda = 1010$ nm, $\lambda = 980$ nm, $\lambda = 920$ nm are excited with plane wave excitation at $\theta = 0^\circ$, and the $\lambda = 850$ nm resonance is excited at $\lambda = 90^\circ$. For all wavelengths,

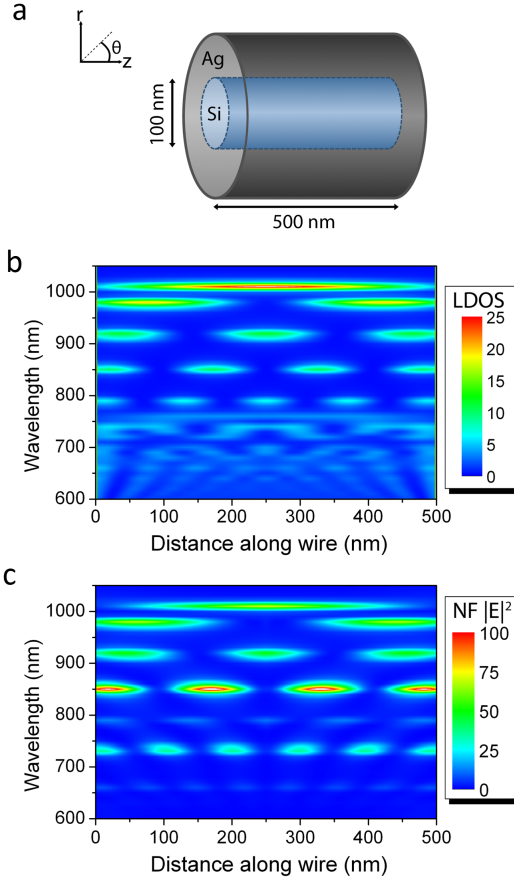


Figure 4.4. Resonant modes for a structure with Si core radius $a = 50$ nm, Ag coating thickness $T = 100$ nm, and length $L = 500$ nm (resonator A). (a) Schematic of this resonator. (b) LDOS as a function of wavelength calculated at a constant radial position of $r = 5$ nm from the center of the Si core, along the length of the wire (0 – 500 nm) with 2.5 nm resolution, and reported with values normalized to the vacuum LDOS. (c) Near field electric field intensity (NF $|\mathbf{E}|^2$) as a function of wavelength calculated from plane wave excitation at an angle of $\theta = 0^\circ$, also at a constant radial position of $r = 5$ nm from the center of the core and along the length of the wire.

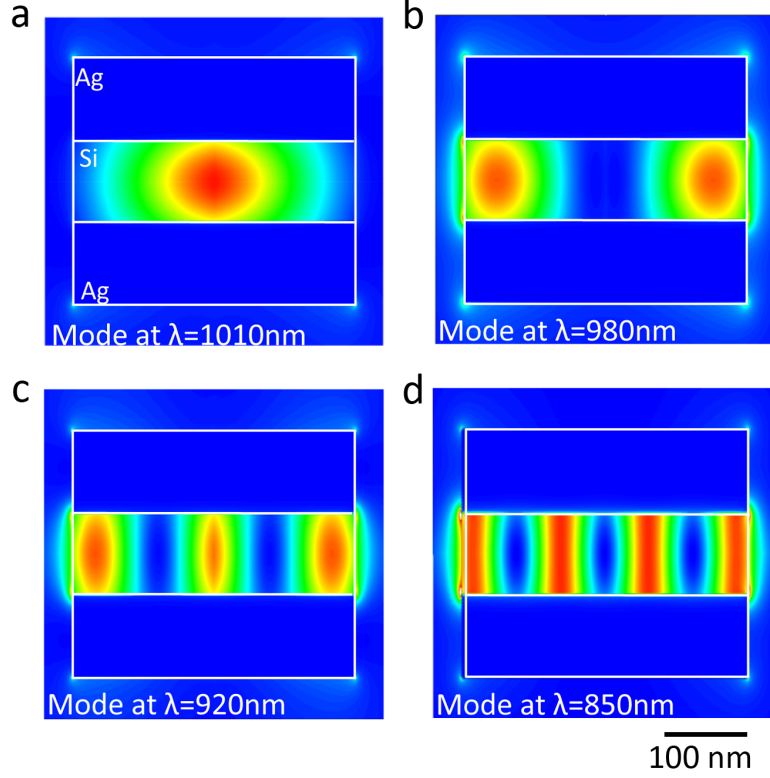


Figure 4.5. Two-dimensional NF $|\mathbf{E}|^2$ profiles for the first four lowest-order longitudinal modes for a structure with Si core radius $a = 50$ nm, Ag coating thickness $T = 100$ nm, and length $L = 500$ nm (resonator A) for excitation at (a) ($\theta = 0^\circ$) $\lambda = 1010$ nm ($\lambda/2$ resonance), (b) $\lambda = 980$ nm (second $\lambda/2$ resonance), (c) $\lambda = 920$ nm (λ mode), and (d) ($\theta = 90^\circ$) $\lambda = 850$ nm ($3\lambda/2$ resonance).

the modes are confined highly within the resonator core. The mode occurring at $\lambda = 850$ nm has the highest NF $|\mathbf{E}|^2$, and $Q = 79$ with a subwavelength mode volume of $V_{\text{eff}} = 0.32(\lambda/n)^3$. This results in a Q/V_{eff} of $247(\lambda/n)^{-3}$.

As expected, upon shrinking the resonator dimensions, modes shift to shorter wavelengths and modes with higher-order azimuthal symmetry are cut off. Figure 4.6 shows the LDOS and NF $|\mathbf{E}|^2$ mode profile for resonator B ($a = 25$ nm, $L = 150$ nm), calculated at a radial position of $r = 5$ nm from the center of the Si core and along the entire length of the resonator. Note the two-fold increase in LDOS as compared to resonator A for the two lowest-order $\lambda/2$ modes ($\lambda = 760$ nm and $\lambda = 700$ nm).

Plane wave excitation at $\theta = 0^\circ$ does excite the first three modes, but the mode at $\lambda = 700$ nm has the improper symmetry to be efficiently excited under these conditions. Excitation at $\theta = 90^\circ$ provides the proper symmetry for this second longitudinal resonance, characterized by high electric field intensity and LDOS at the resonator ends. Note also that the modes at $\lambda = 760$ nm and $\lambda = 700$ nm in this smaller resonator have higher intensity than the modes in the larger resonator A (Figure 4.4).

Figure 4.7 shows both LDOS and NF $|\mathbf{E}|^2$ cross-sectional profiles of the two lowest-order modes of resonator B. The LDOS profiles in Figure 4.7a are calculated only inside the Si core, with the rest of the resonator (Ag coating and surrounding air) shown for clarity. The mode at $\lambda = 760$ nm on the left is characterized by high LDOS in the center of the resonator core, whereas the mode at $\lambda = 700$ nm has high LDOS centered at the resonator ends and is a maximum radially at the Ag/Si interface. The two-dimensional NF $|\mathbf{E}|^2$ profiles for these modes are seen in Figure 4.7b. The mode at $\lambda = 760$ nm is excited with a plane wave at $\theta = 0^\circ$ polarized along an arbitrary radial direction. Strong fields are concentrated in the center of the Si core with high confinement within the resonator and very little penetration into the surrounding medium. Although this resonator is smaller than resonator B, we continue to see high confinement within the Si core. We calculate $Q = 58$ and V_{eff} equal to the physical volume of the Si core, $0.031(\lambda/n)^3$. This results in a Q/V_{eff} of $1870(\lambda/n)^{-3}$. For the second-order mode at $\lambda = 700$ nm, symmetry requires plane wave excitation at an angle of $\theta = 90^\circ$, polarized parallel to the longitudinal axis of the wire (z). The NF $|\mathbf{E}|^2$ profile in Figure 4.7b illustrates high electric fields at the resonator ends, and again little penetration into the metal cladding and surrounding vacuum. This mode has a Q of 53, $V_{\text{eff}} = 0.026(\lambda/n)^3$, and $Q/V_{\text{eff}} = 2040(\lambda/n)^{-3}$. Comparing these numbers to the larger resonator A, we see that smaller resonators continue to exhibit high mode confinement with effective mode volumes approximately equal to the physical volume of the Si core, and lower-order modes do not sustain much loss in quality factor with decreased dimensions. Thus, the figure of merit Q/V_{eff} increases significantly in this smaller resonator.

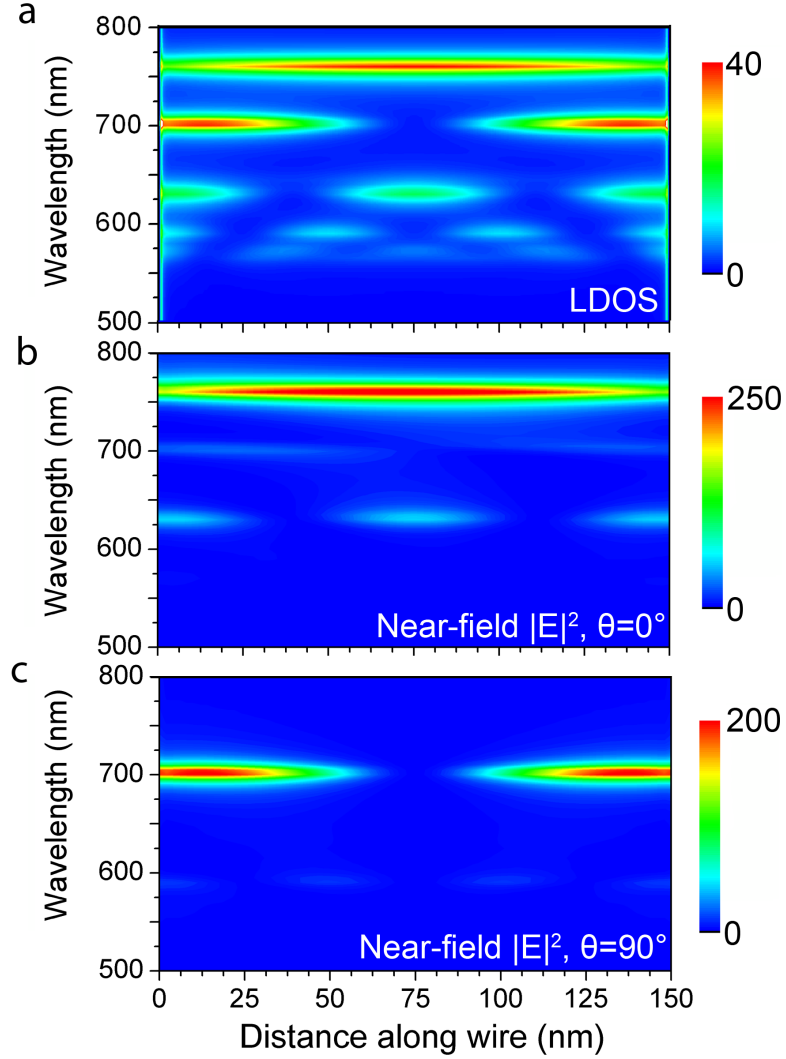


Figure 4.6. (a) LDOS and cross-sectional NF $|\mathbf{E}|^2$ profiles for plane wave excitation at (b) $\theta = 0^\circ$ and (c) $\theta = 90^\circ$ for a structure with $a = 25$ nm, $T = 100$ nm, and $L = 150$ nm. LDOS is calculated at a radial position of $r = 5$ nm from the center with 0.5 nm resolution along the length of the wire and normalized to LDOS in vacuum. NF $|\mathbf{E}|^2$ is also calculated at a radial position of $r = 5$ nm and normalized to the fields of the incident source.

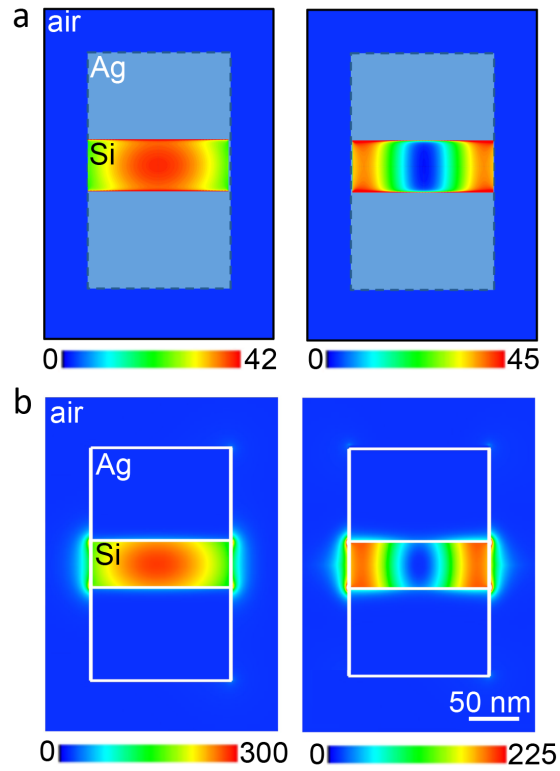


Figure 4.7. Cross sections of (a) LDOS and (b) NF $|\mathbf{E}|^2$ from plane wave excitation at (left) $\lambda = 760$ nm (plane wave excitation at $\theta = 0^\circ$) and (right) $\lambda = 700$ nm (plane wave excitation at $\theta = 90^\circ$).

Continuing to decrease resonator dimensions to the deeply subwavelength resonator C ($a = 5$ nm, $L = 25$ nm), only extremely evanescent modes are supported. As seen in Figure 4.8, the LDOS intensity increases dramatically, as does the NF $|\mathbf{E}|^2$ for plane-wave excitation at $\theta = 0^\circ$. We do not see the traditional longitudinal resonances in the plot of LDOS versus distance along the wire in Figure 4.8a because they are cut off. However, plane wave excitation at $\theta = 0^\circ$ shows a mode at $\lambda = 610$ nm for excitation at $\theta = 0^\circ$. From Figure 4.8c, we can see that the near-field intensity peaks at 4000 times larger than the incident field. This is by far the highest NF $|\mathbf{E}|^2$ of the three resonators studied in detail, and within the smallest resonator volume. Calculating $Q = 26$ and $V_{\text{eff}} = 4.7 \times 10^{-4}(\lambda/n)^3$, we find the highest Q/V_{eff} in this ultra-small resonator at $4.8 \times 10^4(\lambda/n)^{-3}$. Even for such small resonator dimensions, this mode volume is only 16% larger than the physical volume of the Si core with a quality factor that has decreased only slightly from the larger resonators. This demonstrates that upon transition from subwavelength resonators that support true eigenmodes to ultra-small resonators that support only evanescent modes, plasmonic core-shell nanowire resonators with dimensions on the order of $\lambda/50$ are able to confine modes within the physical volume of the resonator core without significant loss in the quality factor.

4.4 Enhancing Radiative Decay

We would also like to determine the light emission properties of the plasmonic core-shell nanowire resonators. An atom can emit or absorb photons by undergoing transitions between its energy levels through any of three specific processes: absorption, spontaneous emission, and stimulated emission [63]. If the atom, approximated as a two-level system with ground state energy E_1 and excited state energy E_2 , is initially in the lower energy level, an electron can be promoted from E_1 to E_2 by absorbing a photon with energy $> E_2 - E_1$. This process is called *absorption*, and can only occur when the radiation mode contains a photon.

An atom in the excited state with an electron in energy level E_2 can radiatively

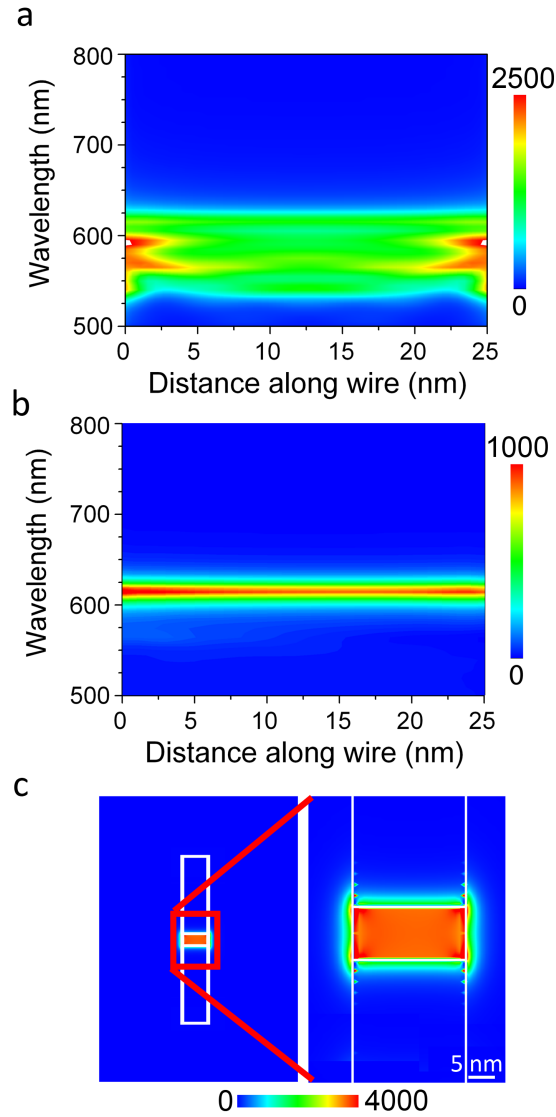


Figure 4.8. (a) LDOS and (b) NF $|\mathbf{E}|^2$ for plane wave excitation at $\theta = 0^\circ$ for a structure with $a = 5$ nm, $T = 100$ nm, and $L = 25$ nm. LDOS and NF $|\mathbf{E}|^2$ are calculated at a radial position of $r = 2.5$ nm with 0.2 nm resolution along the length of the wire. (c) NF $|\mathbf{E}|^2$ cross section for plane wave excitation at $\lambda = 610$ nm and $\theta = 0^\circ$.

decay to the ground state by undergoing either spontaneous or stimulated emission. In *spontaneous emission*, the atom decays to the lower energy state and releases energy in the form of a photon, with energy $E_2 - E_1$. This transition is independent of the number of photons occupying the mode. Alternatively, if the radiative mode already contains a photon, an atom in the excited state can be induced to emit an additional photon into the same mode. This process is *stimulated emission*, and is the inverse of absorption. Here, a preexisting photon with a specific energy, polarization, and orientation induces the emission of an identical photon. This process is the basis of laser operation. There are also nonradiative pathways for decay, such as the emission of phonons.

We are interested in opportunities for enhancing the rate of spontaneous emission. Fermi’s “golden rule” states that the rate of transition between two energy levels is directly proportional to the LDOS [65]. Therefore, by increasing or decreasing the LDOS, one can enhance or suppress the rate of spontaneous emission. This can be achieved in a number of geometries, particularly waveguides [66], antennas [67], and cavities [68].

Edward Purcell in 1946 discovered that the rate of spontaneous emission could be modified when the emitter is placed inside a resonant cavity [69]. This so-called Purcell effect states that the enhancement in the emission rate for maximum coupling is directly proportional to the quantity Q/V , as

$$F_P = \frac{3}{4\pi^2} \left(\frac{\lambda}{n}\right)^3 \left(\frac{Q}{V}\right), \quad (4.4)$$

where F_P , the Purcell factor, is equal to the enhancement of the spontaneous emission rate, λ is the free-space wavelength, n is the refractive index, Q is the quality factor, and V is the mode volume. The Purcell enhancement is illustrated in Figure 4.9. An emitter in free space has a continuum of states available to couple into. When the emitter is placed in a resonator cavity, which supports specific modes due to the boundaries, the rate of spontaneous emission can be modified by coupling into the cavity modes. This enhancement is most significant when the emission wavelength

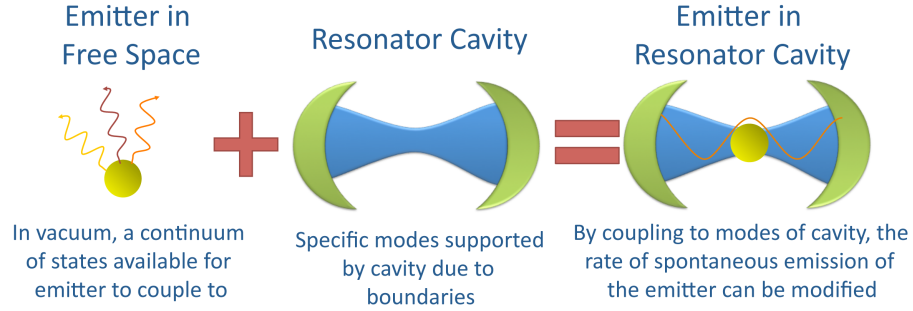


Figure 4.9. Illustration of Purcell enhancement of spontaneous emission in a cavity. A dipole emitter in free space can emit into a continuum of modes, but when placed inside a resonator cavity that supports specific modes, the rate of spontaneous emission of the emitter can be dramatically enhanced or suppressed.

corresponds to the wavelength of a cavity mode and when the emitter is positioned at the field maximum.

Considering (4.4), the maximum enhancement is obtained when Q/V is optimized. This is traditionally achieved by creating resonant cavities with ultra-high quality factors ($Q > 10^6$), but in volumes larger than $(\lambda/n)^3$. In plasmonic cavities such as the core-shell nanowire resonators described in this chapter, modes with low quality factors ($Q < 100$) are confined to subwavelength effective mode volumes V_{eff} and thus can achieve high figures of merit Q/V_{eff} . We have already reported the quality factors and mode volumes for the three resonators A, B, and C, reporting a maximum $Q/V = 4.8 \times 10^4 (\lambda/n)^{-3}$ in the smallest resonator (C).

We also determine what portion of the decay contributes to radiative emission versus absorption by calculating the enhancements in the total and radiative decay rates normalized to Γ_0 , the decay rate in vacuum, given by

$$\Gamma_0 = \frac{4}{3} \frac{|D|^2}{\hbar} \left(\frac{\omega}{c} \right)^3. \quad (4.5)$$

The total decay rate, Γ_{tot} , is related to the LDOS ρ as

$$\Gamma_{\text{tot}} = \frac{4\pi^2\omega|D|^2}{\hbar}\rho. \quad (4.6)$$

Finally, the radiative decay rate, Γ_{rad} , is calculated by integrating the far-field Poynting vector for a dipole source (polarized along r) located inside the Si core of the nanowire.

Results for resonators A, B, and C are shown in Figure 4.10. Peaks in the plot of $\Gamma_{\text{rad}}/\Gamma_0$ correspond to the resonant modes illustrated in Figures 4.4, 4.6, and 4.8. The largest enhancements are seen for the $\lambda = 610$ nm mode of the ultra-small resonator C, with $\Gamma_{\text{rad}}/\Gamma_0 > 13000$. Resonators A and B also see significant enhancements ($\Gamma_{\text{rad}}/\Gamma_0 > 100$ and $\Gamma_{\text{rad}}/\Gamma_0 > 400$, respectively), and both have quantum efficiencies $\Gamma_{\text{rad}}/\Gamma_{\text{tot}}$ of approximately 50%. Remarkably, the smallest resonator C maintains a reasonable quantum efficiency of 26%, again demonstrating the promise of ultra-small plasmonic core-shell nanowire resonators for enhancing the rate of spontaneous emission.

4.5 Core-Shell Nanowire Resonators as Sensors

Enhanced radiative decay suggests using plasmonic core-shell nanowires as molecular sensors. The simplest sensing experiments report a shift in the resonance wavelength when the surrounding medium is changed from air ($n = 1$) to a medium with a higher refractive index, such as water ($n = 1.33$) or sucrose ($n = 1.38$). The figure of merit for sensing is defined as

$$\text{FOM} = \frac{\Delta\lambda}{\Delta n}, \quad (4.7)$$

with units of nm/RIU (refractive index unit) where $\Delta\lambda$ is the shift in resonance wavelength and Δn is the refractive index change. The FOM can also be expressed in units of meV/RIU when

$$\text{FOM} = \frac{\Delta E}{\Delta n}, \quad (4.8)$$

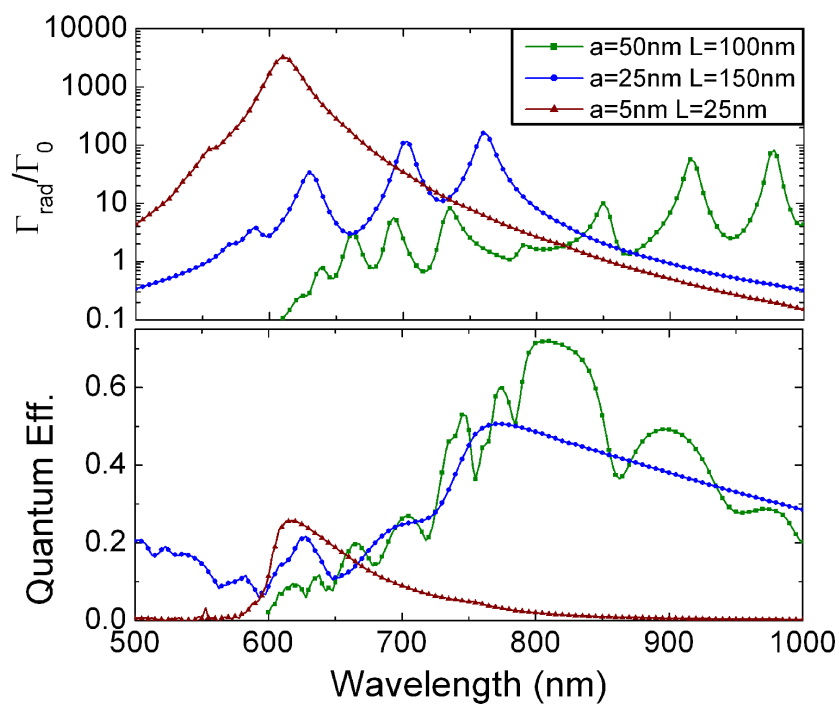


Figure 4.10. Radiative decay rate enhancements (top) and quantum efficiencies (bottom) as a function of wavelength for three different Si-Ag core-shell nanowire resonators. Quantum efficiency is calculated as $\Gamma_{\text{rad}}/\Gamma_{\text{tot}}$.

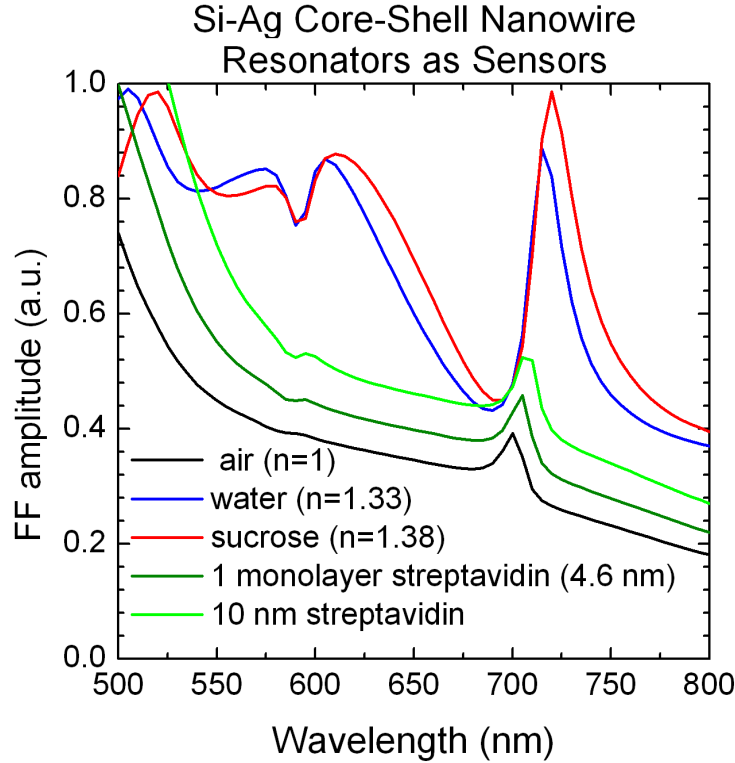


Figure 4.11. Far-field emission spectra for a Si-Ag core-shell nanowire resonator ($a = 25$ nm, $L = 150$ nm) in air ($n = 1$), water ($n = 1.33$), sucrose ($n = 1.38$), and with a single monolayer of streptavidin on one resonator end (4.6 nm) and a 10 nm layer of streptavidin, illustrating how these resonators can behave as sensors.

where ΔE is the shift in resonance energy. This FOM has been calculated for a number of small metal nanoparticles [70, 71, 72], and the metal nanostar demonstrate sensitivities higher than 1000 meV/RIU [73]. For resonator B ($a = 25$ nm, $L = 150$ nm), changes in far-field intensity for plane wave excitation at $\theta = 0^\circ$ for the resonator in air, water, and sucrose is shown in Figure 4.11. Significant spectral changes are observed, not only shifts in the resonance wavelength but also in intensity. When the resonator is situated in a higher index medium, more radiation to the far field is observed. We calculate a FOM for this resonator of 60 nm/RIU or 150 meV/RIU.

Significant effort has been devoted to developing sensors that are sensitive enough

to sense extremely small quantities of analyte, even to the single-molecule level. The biotin-streptavidin system is commonly used in sensing experiments. As a step toward designing single-molecule sensors, we have calculated the far-field emission spectrum for resonator B in air with a single monolayer of streptavidin coating one resonator end (thickness of 4.6 nm), as well as a 10 nm thick layer of streptavidin (Figure 4.11). This thin layer of streptavidin shifts the resonance wavelength and increases the intensity of emission.

4.6 Chapter Summary

In this chapter, we have introduced the Si-Ag core-shell nanowire resonator and performed a thorough investigation of its resonant modes using the boundary element method. A case study of three specific resonators, all with subwavelength dimensions, demonstrated that extremely high modal confinement is observed for all sizes. We calculated the radiative and total decay rates, and saw the most dramatic enhancements for the smallest resonator. A quantitative summary of these three resonators can be found in Table 4.1. Most importantly, we showed that resonators with dimensions on the order of $\lambda/50$ can still confine modes to deeply subwavelength mode volumes without significant loss in quality factor.

Table 4.1. Summary of Q/V and decay rate enhancements in Si-Ag core-shell nanowire resonators

radius a (nm)	50	25	5
length L (nm)	500	150	25
λ (nm)	850	700	610
V_{eff}	$0.32(\lambda/n)^3$	$0.026(\lambda/n)^3$	$4.7 \times 10^{-4}(\lambda/n)^3$
Q	79	53	26
Q/V_{eff}	$247(\lambda/n)^{-3}$	$2040(\lambda/n)^{-3}$	$55300(\lambda/n)^{-3}$
$\Gamma_{\text{rad}}/\Gamma_0$	115	445	13,520
$\Gamma_{\text{tot}}/\Gamma_0$	58	227	3,250
$\Gamma_{\text{rad}}/\Gamma_{\text{tot}}$	49%	50%	26%